On the role of Water-as-Additive in Lithium Electrodeposition

Mark Aarts[a,b], Sai G. Patnaik[a,b], Toon Van Roy[a,b], Stefanie Sergeant[c], Maarten Debucquoy[a,b], Philippe M. Vereecken[a,b]

[a] imec, Energy Department, Kapeldreef 75, 3001 Leuven, Belgium

[b] Energyville, Thor Park 8310, 3600, Genk, Belgium

[c] imec, Department of Material and Component Analysis, Kapeldreef 75, 3001 Leuven, Belgium

Electroplating of flat and smooth lithium layers is key for batteries using metallic lithium as the anode, where a major failure mechanism is the self-enhancing uneven or ramified growth of lithium metal leading to capacity fading or even short-circuiting during cycling. In that regard we shed new light on an intriguing growth mode for electrodeposited lithium in this work, where lithium self-assembles in a compact columnar morphology. Such growth results in topographically smooth layers and a particular stripping behavior along the length of these nanorods, rather than from the top down. Here, we demonstrate the electroplating of smooth layers of columnar lithium using LiTFSI and $LiClO_4$ salts, which rules out the commonly found explanation of a LiF interface layer directing growth. Rather, we find that the addition of water to these (non-hydrolising) electrolytes is key for the guided growth. We investigate its effect both during electrochemical formation (applied potentials > Li^+/Li), and growth (applied potentials < Li^+/Li), and observe that the presence of water is required during the whole process. We use a rotating ring disk electrode (RRDE) to study the process *in-situ*, and find that hydrogen is continuously generated. Notably, hydrogen is generally considered as a side-product in the LiF based mechanism, and we therefore suggest that the evolution of hydrogen is in fact the critical component for the directed growth. Such an explanation homogenizes our results with earlier reports and provides mechanistic insights for the role of water during lithium electrodeposition, which is invariably present in lithium metal batteries.

Introduction

Control over the morphology of lithium metal during electrodeposition has become a major topic in battery research[1], with many works focusing on the stability of the lithium metal anode over repeated electroplating and stripping cycles[2–5]. Cycling and subsequent observation, typically done using scanning electron microscopy (SEM), does not always provide the full picture however, as illustrated in literature by recent mechanistic insights obtained using a variety of additional techniques to study the growth of lithium metal[6–12]. Furthermore, the wide range of electrolyte systems used[13] makes it difficult to compare results between different reports or to disentangle physical[14] and chemical[15] effects responsible for uncontrolled lithium growth. Growth of smooth lithium morphologies attributed to electrostatic shielding for example[16], was later found to consist of a particular self-aligned and compact nanorod morphology[17].

Such a columnar morphology is very similar to the results first obtained by Kanamura et al.[18] using HF as an additive, and later with trace amounts of water for the *in-situ* formation of HF through the hydrolysis of an $LiPF_6$ electrolyte[19]. This growth mode is commonly attributed to the formation of a LiF solid electrolyte interphase (SEI) layer mainly based on X-ray photoelectron spectroscopy[20–22]. So far, deposition of columnar lithium layers has attracted

interest for its smooth or 'dendrite-free' morphology, but has also shown improved results in terms of lifetime[23] and Coulombic efficiency[24]. In particular, a unique plating and stripping along the length of the columns has been observed in cycling[17,25,26] implying reduced local current densities and limited volumetric change of the lithium metal anode, mitigating well-known causes of ramified lithium growth and failure in lithium metal batteries.

Recently however, questions have been raised about the role of LiF in the growth of columnar lithium[27], with similar structures also being observed in (non-hydrolysing) LiTFSI[22] and $LiNO_3$[28] electrolytes. As the bulk of the aforementioned references advocate the formation of a LiF rich SEI mediated by HF present in the electrolyte as the cause for columnar growth, a more complete understanding of the mechanism responsible for columnar lithium growth is required for further optimization for lithium metal anodes.

In this work we demonstrate the electroplating of columnar lithium morphologies obtained directly with water-as-additive. We achieve these columnar layers using both non-hydrolysing LiTFSI, and fluorine-free $LiClO_4$ electrolytes, unambiguously proving that a LiF-rich SEI cannot be considered as the determining factor for this growth mode. We investigate the role of the formation step (i.e. electrochemical reactions occurring at potentials above the lithium deposition potential), an alternative hypothesis from literature, using *ex-situ* Atomic Force Microscopy (AFM) in a glovebox environment and electrochemical experiments. We find that such a formation layer does not account for our experimental results, but the water rather has a continuous role during the growth. We demonstrate that the process of columnar growth can be controlled by balancing the concentration of added water to the deposition rate. Finally, we use a rotating ring disk electrode (RRDE) to study the growth process *in-situ* and find that hydrogen is continuously evolved during Li growth. Considering that a mechanism which is independent of the anion is required based on our results (as both LiTFSI and LiClO4 give similar results), we therefore suggest that the continuous presence of hydrogen is the determining factor in obtaining the columnar lithium morphology. As hydrogen is also reported as a product in the electrocatalytic formation of LiF in electrolytes containing HF, such an explanation homogenizes our results with existing literature and provides mechanistic insights for the design and control of lithium metal morphologies.

Results

Columnar lithium electroplating

Lithium electrodeposition experiments were carried out in a 3-electrode cell, using a copper substrate as working electrode (150 nm copper + 10 nm titanium sputtered on a silicon wafer, Si-Mat), and metallic lithium as counter-, and quasi-reference electrode (QRE). All potentials in the remainder of the text are versus the Li QRE. We use tetraethylene glycol dimethyl ether (4G) as a solvent, which was selected mainly based on the high boiling point and the electrochemical stability of ether solvents[29]. The solvent was dried over 4 Å molecular sieves, after which 1 M LiTFSI and 1 M $LiClO_4$ electrolytes are prepared with varying amounts of water as additive.

Figure 1 shows scanning electron microscopy images (SEM) of the resulting lithium layer, after galvanostatic electrodeposition at -1 mA/cm^2 up to 0.74 C/cm^2 (expected to yield 1 µm of electroplated lithium at 100% Faradaic efficiency) for both salts at different concentrations of the water additive. The insets of the figure show digital photos of the sample after rinsing with anhydrous Propylene Carbonate (PC) and vacuum drying. It is clear from the figure that the morphology of the deposit is governed by the concentration of the water additive and that the deposition qualitatively follows the same trend irrespective of the used salt, going from a mossy, to a columnar morphology. The essential role of water, rather than the salt, is also apparent in the color progression of the samples, which evolves from grey/black, to blue, to yellow in both cases. In fact, we will show later that the presence of water is a prerequisite, as we find that there is no adhesion for the deposit in the case of the fully dry solvent.

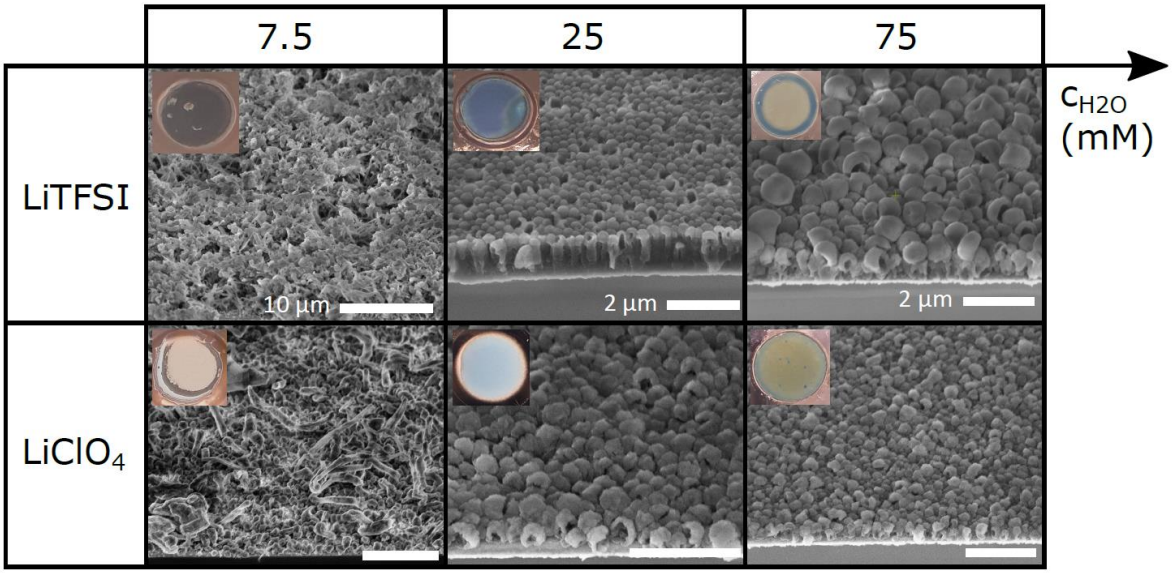

Figure 1: SEM images (45° sample tilt) of samples after galvanostatic electrodeposition at -1 mA/cm^2 until reaching -0.74 C/cm^2 using 1M LiTFSI and $LiClO_4$ salts and various concentrations of the H_2O additive. Insets show digital photos of the samples. Columnar morphologies are observed for both salts, with the same progression of morphology and sample color. The scale bars are the same in both rows.

Additional (cross-sectional) SEM, atomic force microscopy (AFM) images, and V-t traces of these experiments are provided in SI-1, where we note that it was more difficult to grow from the $LiClO_4$ than from the LiTFSI electrolyte. As this typically results in black spots that wash away with the PC rinse and a thinner layer than expected based on the total passed charge, we focus on the LiTFSI salt in the remainder of the paper.

The results in Figure 1 are in stark contrast with the prevailing explanation of HF-mediated formation of LiF being responsible for columnar growth, where LiTFSI is often used as a reference salt resistant to hydrolysis, and does not yield columnar structures[15,19,24]. It is worth pointing out that we obtain the same results even when using the electrolytes directly after preparation, as a > 48 h waiting period after the addition of H_2O is typically required for the formation of HF in $LiPF_6$ based electrolytes[19,27,30]. The columnar morphologies obtained from LiTFSI and the fluorine-free $LiClO_4$ electrolytes are therefore a key result, as it rules out such a mechanism being responsible for this particular mode of growth. Figure 2a shows that layers

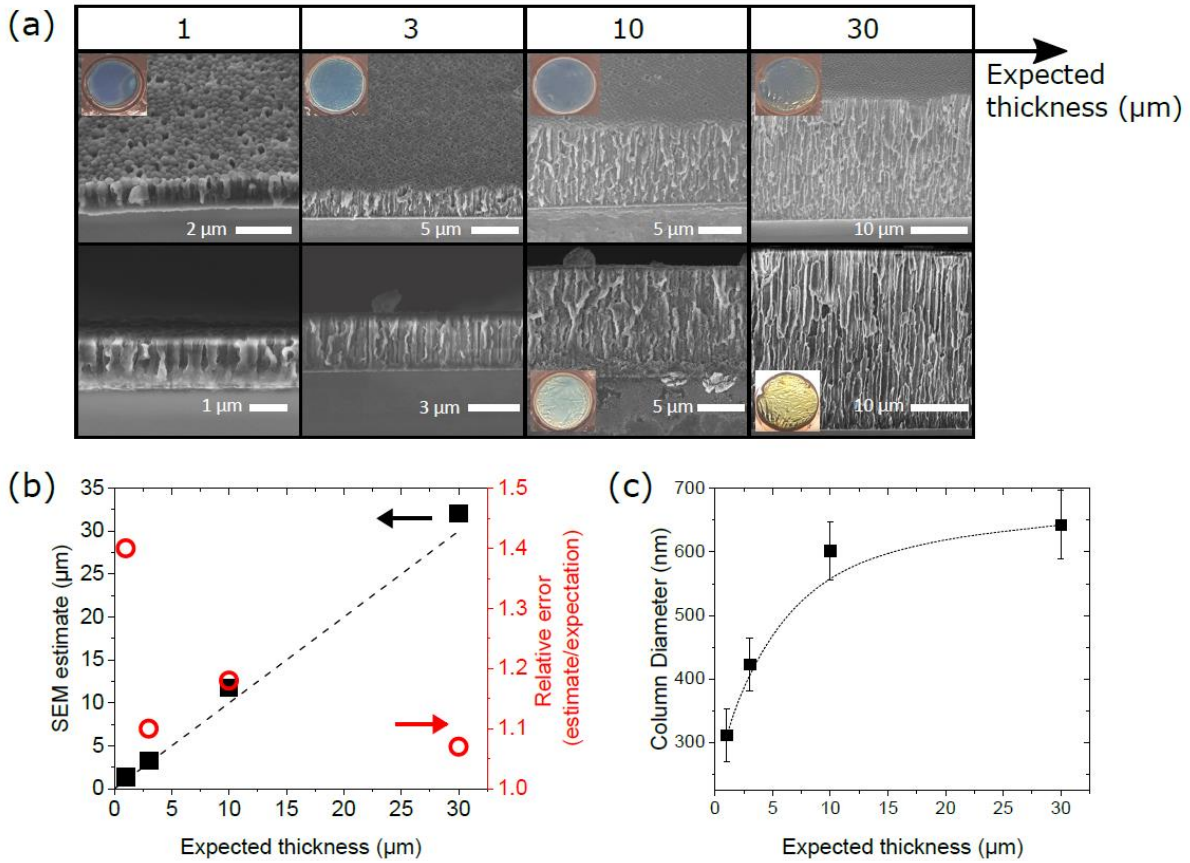

Figure 2: *(a) SEM images of layers deposited galvanostatically from 1 M LiTFSI + 25 mM H_2O (4G) at -1 mA/cm^2 for various expected layer thickness (from equivalent charge). Top row: 45° sample tilt. Bottom row: ~90° sample tilt. Insets show digital photos of the substrates. (b) Layer thickness estimated from SEM, as a function of the expected plating thickness. The dashed line is expectation = estimate. The right y-axis is the relative error, decreasing as a function of plating thickness. (c) Estimated column diameter as a function of plated thickness, saturating at ~600 nm. The line is a guide to the eye.*

of arbitrary thickness can be grown from the LiTFSI salt with 25 mM of H_2O at a current density of -1 mA/cm^2, which we control by means of the plating duration and is demonstrated here for layers up to 30 µm (~-21.6 C/cm^2). The insets again show digital photos of the samples, where we note that a pronounced angular dependence of the reflection becomes apparent for thicker layers (top images, tilted, bottom images, perpendicular). From the SEM images we further estimate the thickness of the layer (Figure 2b) and the diameter of the columns (Figure 2c) as a function of the plating time. We observe that the relative error of the measured height decreases over time, as compared to the height expected from the equivalent charge, yielding a relative error < 10% for the thickest layer, while the column diameter increases with the layer thickness but saturates at ~600 nm. This seems to imply that the layer initially has some voids, which close through expansion of the column diameter over time. Based on these results we typically electrodeposit -7.4 C/cm^2 (equivalent to 10 µm of lithium) in the remainder of the text.

Having demonstrated that water-as-additive yields a similar morphology to strategies based on the *in-situ* formation of HF, we turn our attention to potential mechanisms responsible for the columnar growth mode. In particular, we independently looked at the formation step (i.e. electrochemistry occurring at potentials above the thermodynamic lithium deposition potential, or 0 V vs. Li QRE), and the growth step. Here, there appears to be ambiguity in literature with some reports stating that the formation step is critical[23,24,27], and others emphasizing the importance of continuous stirring (or continuous supply of the additive) of the electrolyte during growth[25,31,32].

Formation versus growth.

As a first step to study the effect of the formation, we consider the hypothesis from Kasse et al[27] that the physical nanostructure, rather than the chemistry, of the formation layer guides the growth. Their hypothesis is based on the similarity of XPS results of samples with-, and without use of the additive. To examine this, we prepare the surface by keeping the working electrode at a certain potential until a total charge of -10 mC/cm^2 is achieved, which is approximately the total charge before the onset of lithium nucleation in our galvanostatic electrodeposition (SI-1). After this formation step, the sample is rinsed with anhydrous PC, dried in vacuum, and the surface is characterized using AFM. The AFM is situated inside an

N_2/Ar glovebox and samples are transported in sealed vessel to ensure that the surface is not affected by exposure to ambient air.

To find the potentials of interest, linear sweep voltammetry (LSV) from open circuit potential (OCP) to 0.1 V vs. Li QRE at 5 mV/s is shown in Figure 3a for different concentrations of the H_2O additive. We note that there are 2 peaks that *systematically* change with the water concentration, i.e. the reaction at ~1.3 V, which increases with increasing the amount of water, and the reaction at ~1.7 V, which increases and shifts to ~1.95 V (SI-2). We note here that the current density of these peaks is still a few factors smaller than those typically found for the electrochemical reduction of (100 ppm of) HF[19,27,30]. The behavior of both these peaks is consistent with the results of Aurbach et al.[33] upon the addition of water, where it should be noted that in that work the peak around ~1.7 V was also affected by the presence of oxygen (see methods). The inset of Figure 3a shows a cyclic voltammogram (CV) at 5 mV/s for 10

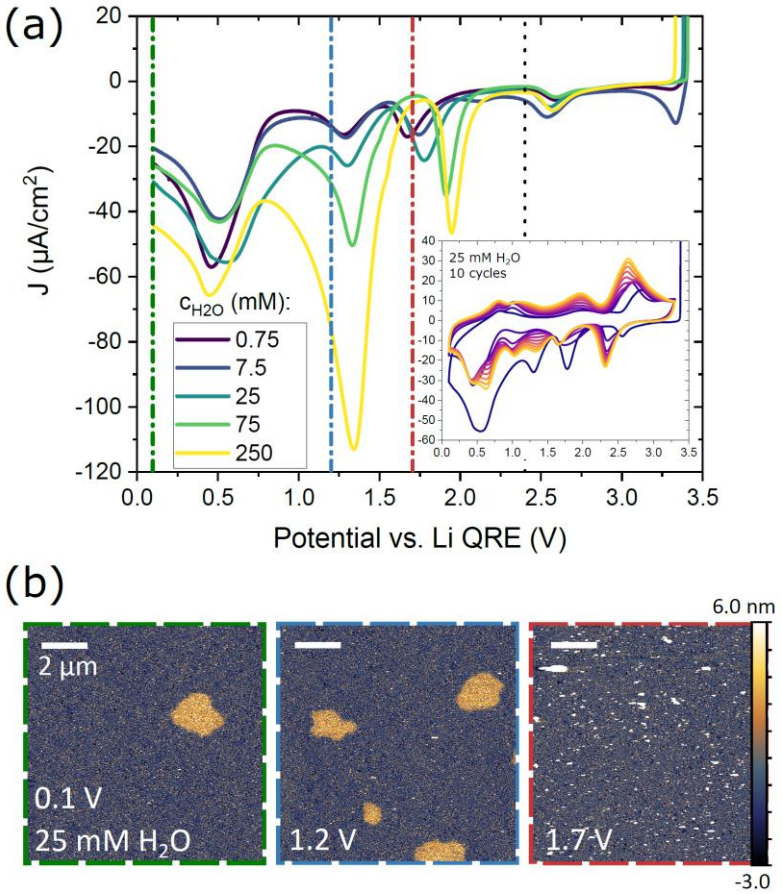

Figure 3: *(a) LSV at different concentrations of the H_2O additive from open circuit potential to 0.1 V vs. Li QRE. The scan rate was 5 mV/s. Dashed lines indicate potentials where samples were prepared for ex-situ AFM (SI-3 for the black line). The inset shows a CV (10 cycles, from purple to orange) with 25 mM H_2O at 5 mV/s, using the same axes. (b) ex-situ AFM images of samples held at 0.1, 1.2, and 1.7 V (green, blue, red outline, respectively) until reaching the charge setpoint of -10 mC/cm^2. Scale bars are 2 µm.*

cycles for the 25 mM electrolyte. Strikingly, we observe that the peak at ~1.3 V is passivated in the second cycle, as in reference[33], but reappears and splits in subsequent cycles.

Based on the LSV, we prepare samples with electrolyte containing 25 mM H_2O at different potentials, as indicated by the dashed lines. AFM topography images are shown in Figure 3b for samples prepared with the 25 mM H_2O electrolyte, and kept at 0.1, 1.2, and 1.7 V vs. Li QRE until reaching -10 mC/cm^2, respectively (green, blue, and red dashed outline). Topography images for samples kept at 2.4 V and from a dry (reference) electrolyte are shown in SI-3, where little to no features were observed. At 1.7 V the surface is seeded with particles of ~10s of nm in height and ~50-100 nm in width. At lower potentials the most notable feature are islands of a few micron wide, but only ~3 nm high, that show a remarkable similarity to so-called 'micropancakes', typically associated with trapped gas in a liquid environment[34,35]. In particular, we observe that the density of these islands was highest for the sample kept at 1.2 V in the 25 mM H_2O electrolyte, by more than an order of magnitude compared to the sample kept at 0.1 V and the dry references (Table SI-3). While none of these features can be linked directly to the columnar deposition due to their sparsity and size, these islands appear to originate from the reduction process at 1.3 V in the presence of water.

Secondly, as we do not observe a clear nanostructure responsible for columnar lithium with AFM, we replicate the experiment by Kasse et al.[27]. To study during which part of the electrodeposition the additive plays a role, the working electrode is prepared in the electrolyte with the 25 mM H_2O additive (wet electrolyte), after which the cell is rinsed, and the electrolyte is replaced with the dry electrolyte at different times during the electrodeposition process. The cell is rinsed 2 times with the dry electrolyte during the solvent exchange and all experiments are done galvanostatically at -1 mA/cm^2, up to a total charge of ~-7.4 C/cm^2. The resulting morphologies as observed by SEM and digital photos are shown in Figure 4a-c after rinsing the samples with anhydrous PC and vacuum drying, with the corresponding V-Q traces depicted in Figure 4d. The arrows indicate at what point the dry electrolyte is introduced. First, Figure 4a shows the result when only the dry electrolyte is used (dry at 0 mC/cm^2, green trace). Notably, in this case we observed that there was no adhesion between lithium and the substrate and only small amount of material was present on the substrate. Second, Figure 4b and Figure 4c depict samples where the dried electrolyte is introduced after respectively bringing the sample down to 0 V galvanostatically (dry at -7.2

mC/cm^2, blue trace), and after completing half the process (dry at -3.7 C/cm^2, red trace) in the wet electrolyte at -1 mA/cm^2. It is worth pointing out that the V-|Q| trace shows no noticeable difference between the formation in the dry and the wet electrolyte. Figure 4b shows that formation in the wet electrolyte enables adhesion of the deposit to the substrate but does not result in a columnar morphology. A similar experiment with a longer formation step at 0 V yields the same result (SI-4). This result therefore indicates that the formation affects the growth of lithium by means of the adhesion to the substrate, but that the additive also continuously plays a role during the growth. The continuous need for the additive to direct the growth is even more evident from Figure 4c, where the columnar morphology switches to a non-directed mossy growth immediately upon exchange of the solvent.

Our results appear to be in direct contrast to the ones from Kasse et al.[27], where a columnar morphology is obtained with electrolyte replacement after galvanostatic cycling to 0 V. We rationalize this difference by the fact that an LP30 (1 M $LiPF_6$ in EC/DMC) electrolyte was employed in their case. It is known that the *in-situ* hydrolysis of $LiPF_6$ and associated HF

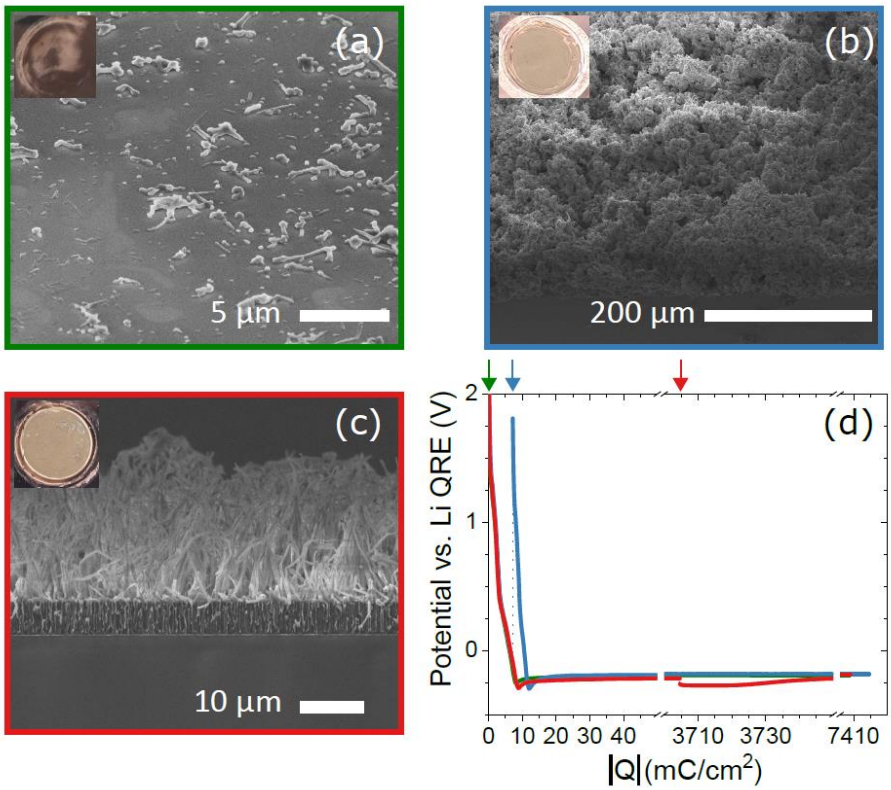

Figure 4: *(a-c) SEM images ((a-b) 45°, (c) 90° sample tilt) after galvanostatic electroplating -of 7.4 C/cm^2, when replacing the 1 M LiTFSI + 25 mM H_2O (4G) electrolyte by the dry 1 M LiTFSI (4G) electrolyte after varying total charge. Insets show digital photos of the substrates. (a) Using only dry electrolyte (at 0 mC/cm^2) result in no adhesion of lithium to the substrate. (b) Introducing the dry electrolyte after galvanostatic cycling to 0 V (-7.2 mC/cm^2) results in mossy growth. (c) Exchanging the electrolyte after completing half the plating (3.7 C/cm^2) results in 5 µm of columnar growth, and switches to a non-directed growth mode immediately upon solvent exchange. (d) V-|Q| traces of the plating, arrows indicate where the dry electrolyte was introduced.*

formation already results in smooth/columnar morphologies at trace amounts of the H_2O additive as low as 25-50 ppm (resulting in double the amount of HF)[19]. In our experiments on the other hand, we add approximately an order of magnitude more water (~450 ppm at 25 mM H_2O). We therefore believe that our electrolyte system provides much finer control over the process, which is in line with the observation of the reduced current density in Figure 3a, as compared to HF containing electrolytes. Along this line, it is worth pointing out that the 'wet-formation' morphology shown in Figure 4b is very similar to the one obtained with the as-received LP30 electrolyte, without any additive, in reference[27].

Finally, we show that columnar morphologies are obtained when scaling the additive concentration with the plating current density in Figure 5a and 5b. Plating is conducted up to a total charge of -7.4 C/cm^2, both when using 7.5 mM H_2O at -0.3 mA/cm^2, and 75 mM H_2O

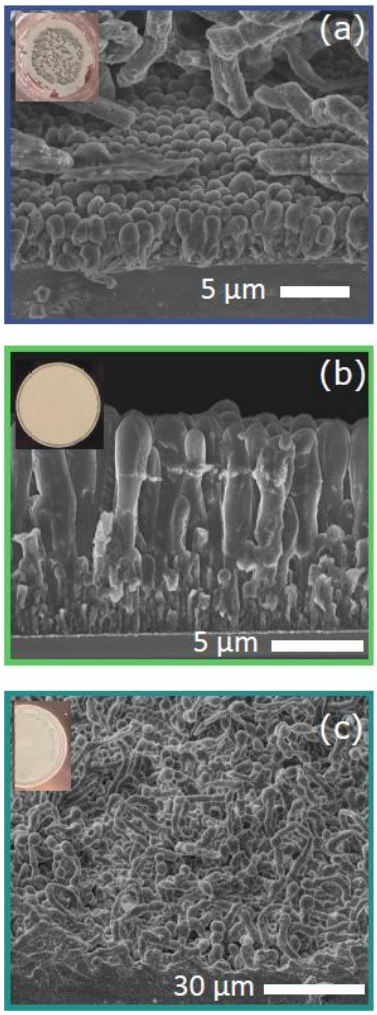

Figure 5: *SEM images after galvanostatically electroplating -7.4 C/cm^2 from 1 M LiTFSI, using various current densities and concentrations of the H_2O additive. Insets shows digital fotos of the substrates. (a) 7.5 mM H_2O at -0.3 mA/cm^2 (45° sample tilt). (b) 75 mM H_2O at -3 mA/cm^2 (90° sample tilt). (c) 25 mM H_2O at -3 mA/cm^2 (45° sample tilt).*

at -3 mA/cm^2, respectively. Columns are observed underneath large patches of more irregular growth for the former (Figure 5a), while smooth columns of the expected height are seen for the latter conditions (Figure 5b). It is worth pointing out that in both these cases the column diameter is much larger than for the conditions used in Figure 2, such that the samples did not display any bright colors. Furthermore, a poorly directed mossy growth is again obtained when increasing the current density to -3 mA/cm^2 in the electrolyte with 25 mM H_2O, shown in Figure 5c, where a more complete sweep of the experimental space is provided in SI-5. Taken together, these results qualitatively suggest that the rate of lithium deposition has to be balanced by supply of the additive to obtain the directed columnar growth.

Rotating Ring Disk Electrode

To further investigate the growth process we use a rotating ring disk electrode (RRDE) with a Cu disk (A_{disk} = 0.196 cm^2) and a Pt ring electrode, with a collection efficiency of 25.6%. The ring potential is fixed at 3.5 V, which is expected to be sensitive only to molecular hydrogen[36], and the electrode is rotated at 100 rpm. Figure 6a shows the response of the ring current as the disk potential is cycled at 5 mV/s from OCP to 0.1 V at different concentrations of added water. We note however that a greyish deposit was observed on the disk after subsequent electroplating for the dry electrolyte (SI-6), such that this case might not be comparable one to one with the stationary electrode (Figure 4a and methods). The disk current shows similar features to what was observed on the stationary electrode in Figure 3a. The ring current concurrently displays clear peaks at ~0.5 and 1.3 V, with a minor increase near 2 V. Furthermore, both the disk and the ring current at 1.3 V increase with increasing water concentration, while at the 0.5 V peak they are both highest for the dry electrolyte. It is worth mentioning that the same behavior was observed when using a $LiClO_4$ salt (SI-6). To understand the voltammogram it is insightful to consider the fraction of the current generating hydrogen at the disk, or efficiency, by plotting $\left|\frac{I_{ring}}{I_{disk}*0.256}\right|$, as shown in Figure 6b for the downward scan. As this representation is sensitive to noise at low I_{disk} we mainly consider the positions around the peaks in disk current, indicated by the arrows. As such, the first (2 V) peak actually results in a dip in the partial current, which corresponds to a H_2 generating partial current of ~0.1 for both 25 mM, and 75 mM of added H_2O. At the second (1.3 V) peak, the partial current is clearly dependent on concentration of H_2O, rising to

approximately half the total current at the highest concentration. Importantly, the efficiency plateaus with a slight decrease as the scan progresses, indicating that all reactions passivate at similar speeds. The observation of the plateau is also crucial at 0.5 V. In fact, while a peak is observed in the ring current, the efficiency dips before recovering. As such, we do not

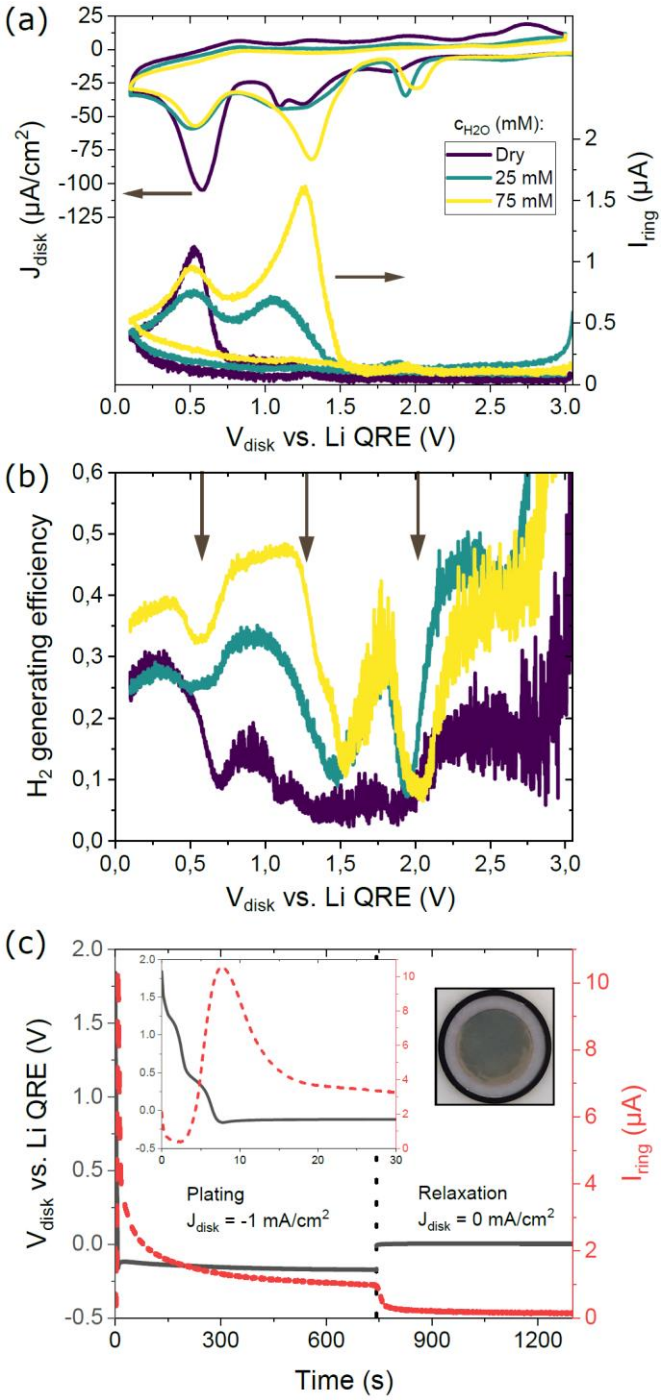

Figure 6: *(a) CV of the Cu disk from OCP to 0.1 V with the Pt ring kept at 3.5 V for different concentrations of the H_2O additive. The disk current density (top, left axis), and absolute ring current (bottom, right axis) are shown. The scan rate is 5 mV/s. (b) Partial current density obtained from (a) (see text) for the first downward scan. The arrows indicate the peaks in disk current, taken from the 75 mM trace. (c) Galvanostatic plating (black, left axis) on the disk at -1 mA/cm^2, with the ring at 3.5 V (red, right axis). After electroplating of 1 µm Li the disk current density is switched to 0 mA/cm^2, with the ring kept at 3.5 V. The left inset shows a zoom-in of the nucleation (first 30 s). The right inset shows a photo of the RRDE after the process.*

attribute the peak in ring current to an additional H_2-generating reaction, but rather to be due to a different process that catalyses the reaction starting at the 1.3 V peak. As the peak at 0.5 V is typically associated with Li underpotential deposition (UPD) process[33], this can potentially be attributed to modification of the surface. We therefore consider 2 reactions generating H_2, with onsets near ~2 V and ~1.3 V.

The absence of ring current in the return trace indicates that both these reactions are passivating however, as also observed over multiple cycles (SI-6). We therefore turn our attention to the ring current during the electroplating in Figure 6c, where galvanostatic growth of ~1 µm of lithium on the disk at -1 mA/cm^2 on the disk is followed by relaxation at 0 mA/cm^2, while keeping the ring at 3.5 V. This protocol also resulted in a blue color of the electrode, similar to the stationary case, as shown in the right inset. In contrast to the vanishing ring current during CV however, hydrogen is continuously detected during growth, and rapidly decays (over a period of ~30 s) when the process is stopped. A large peak in the ring current is seen at the time of nucleation, as depicted in the left inset which decreases towards a steady state current (where an I_{ring} of 1 µA corresponds to 0.05 partial current). These figures seem to imply that fresh lithium is required for the generation of hydrogen. This is based both on the vanishing ring current during prolonged formation (cycling) and relaxation after growth (where the disk potential is 0 V), and on the peak in ring current during nucleation and early growth, where the growing layer is expected to have the largest surface area[37,38]. We further note that the generation of hydrogen is not limited by diffusion, based on the effect of H_2O concentration and rotation rate (SI-6). Importantly, these results also indicate that hydrogen is continuously present at the interface during the electrodeposition process.

Discussion

Following our results, a potential mechanism responsible for the growth of columnar lithium morphologies should (i) rely on the water additive, (ii) be independent of the anion, and (iii) be acting continuously during growth (as opposed to during formation only). Following (i), we examine the 2 water dependent reactions (Figure 2a), that were both found to generate H_2 (Figure 6a,b). Possible reactions meeting the criteria are [39,40]:

$$2H_2O + 2e^- \rightarrow 2\,OH^- + H_2 \qquad U_0 = 2.21\ \text{V vs. } Li^+/Li \qquad (1)$$

$$2H_2O + 2Li^+ + 2e^- \rightarrow 2LiOH + H_2 \qquad U_0 = 2.09\ \text{V} \qquad (2)$$

$$H_2O + 2Li^+ + 2e^- \rightarrow Li_2O + H_2 \qquad U_0 = 1.68\ V \qquad (3)$$

With standard potentials calculated from the change in free energy (SI-7). For the first reaction (peak at 1.7-2 V) we note that the H_2 partial current was only ~0.1. Considering the AFM images (Figure 2b) after holding the potential at 1.7 V, this corresponds to -1 mC/cm^2 for the hydrogen generating reaction. Strikingly, the expected volume of LiOH or Li_2O for this amount of charge following reaction (2) or (3) is ~0.17 µm^3 and ~0.08 µm^3, respectively, where we obtain a very similar value of 0.065 µm^3 from the AFM images. We therefore consider it likely that the observed particles are either LiOH and/or Li_2O, which have also previously been observed in our electrolyte system[41]. We emphasize that this does not rule out the formation of additional (potentially corroding) Lithium or organic species (SI-7), as a large part of the total current remains unaccounted for. For the second reaction (peak at 1.3 V) no particles are observed in Figure 2b. In fact, the total volume of the patches after holding at 1.2 V is ~0.018 µm^3, despite the partial current being > 0.3 at this concentration of the H_2O additive, which would result in a larger volume of material following reactions (2) or (3). We therefore attribute this peak to the hydrogen evolution reaction (HER), reaction (1), similar to what was argued in a LP30 electrolyte[30].

Analogously, we further assume (iv) that the mechanism is the same for HF rich electrolytes and our water-based process due to the evident similarity of the resulting layers which in the former is ascribed to the electrochemical reduction of HF[19,30]:

$$2HF + 2Li^+ + 2e^- \rightarrow 2LiF + H_2 \qquad U_0 = 3.22\ V \qquad (4)$$

We note that the expected standard potential of reaction (4) is 1 V higher than that of reaction (1), which we observe near ~1.3 V, and it is also typically found at ~2.3 V[19,30,36]. Following the discussion and criteria above, it becomes apparent that H_2 is the only common denominator between the HF-based and the water-based process, where the RRDE results additionally show that hydrogen is continuously generated during growth. Taken together, this leads us to believe that H_2, rather than LiF, is the critical component for columnar lithium growth, which is the main result of this paper.

Based on this we put forth two potential mechanisms through which H_2 guides growth. Firstly through the continuous formation of a LiH surface layer. (Electro)chemical conversion of Li to LiH is possible in the presence of hydrogen and has been directly observed recently[7,42]. While

we cannot verify the presence of LiH through our experiments, a LiH surface layer has previously been found to direct growth[6] and is consistent with our results, as we consider the presence of hydrogen to be critical.

Secondly, we recognize that the previous mechanism does not account for the closely packed template of the layers. Inspired by the micropancake topography shown in Figure 3b, typically found in the field of surface nanobubbles[43], we hypothesize that a hydrogen nanobubble template could result in the observed columnar growth. Electrodeposition on bubbles has been demonstrated in the past[44], even resulting in similar nanowire morphologies[45,46]. We further note that this is consistent with some of the columns appearing open/hollow (Figure 1, SI-1, and SI-8), and the template being volatile and therefore not observed in *ex-situ* AFM. Despite not observing any templated surface structure, it is worth mentioning that we were able to tune the column diameter through prolonged formation times at 0 V (SI-8).

Our results are summarized schematically in Figure 7. During formation at potentials V > Li^+/Li, Figure 4a,b indicate that a layer promoting Lithium adhesion forms under influence of the H_2O additive. Following the discussion above we therefore consider this layer to likely consist of Li_2O, LiOH and possibly LiH species (after Li UPD), with HER occurring simultaneously (Figure 7a). During growth, at potentials V < Li^+/Li, growth is directed under influence of the H_2O additive through HER (Figure 4c), such that all these species are likely to be present in the nanorod shell (Figure 7b). It should be stressed that we consider this to be a highly dynamic process, also illustrated by the fact that the additive concentration has to be balanced with the growth rate (Figure 5, SI-5), where these species can be converted further after formation (SI-7)[39–41].

Finally, we comment on the characteristics of the electrodeposited layers. Similar to other authors[17,19,22] we find a rather unique stripping behavior where the columnar (shell) structure

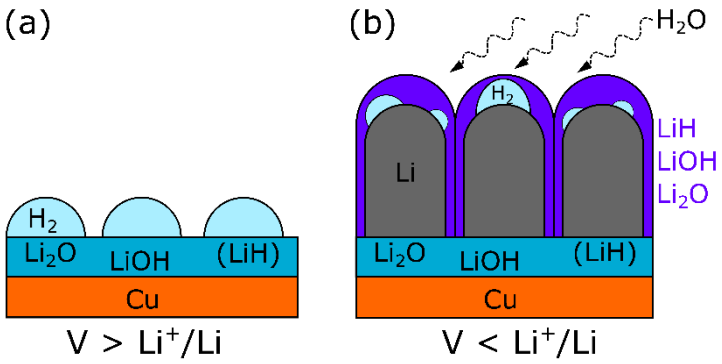

Figure 7: *Schematic representation considering the relevant species formed under influence of the H_2O additive. (a) Above 0 V vs. Li^+/Li a layer facilitating Li adhesion is formed and H_2 is generated. (b) During growth all previous reactions can occur simultaneously, which direct the columnar growth when the additive concentration is balanced with the growth rate.*

remains fully intact. This implies that stripping occurs along the length of the columns, which amounts to a greatly enhanced surface area compared to the geometrical footprint (SI-9, after stripping 3.8 C/cm^2 from a 10 µm layer (~50%) at a current density of ~4.5 mA/cm^2). Reversible plating/stripping in such a manner therefore implies highly reduced local current densities, and mitigates issues regarding volumetric contraction/expansion of the layer.

Conclusion

In conclusion, in this paper we demonstrate the growth of columnar lithium layers up to 30 µm in thickness, through the use of water as an additive. We show that this morphology can be grown using both non-hydrolysing (LiTFSI) and fluorine-free ($LiClO_4$) electrolytes, proving that a LiF SEI derived from electrolytes containing HF cannot be considered as the governing factor for this growth mode, as is often advocated in literature. Furthermore, we test an alternative hypothesis that relies on the formation step (potentials above 0 V vs. Lithium) for the columnar growth and find that this is also not consistent with our results. Rather we find that the water additive plays a continuous role in guiding the electroplating and should be balanced with the deposition rate. Finally, we investigate the growth process using a rotating ring disk electrode and observe that hydrogen is continuously present during growth. Based on these results we consider molecular hydrogen to be the critical component for columnar lithium growth, which homogenizes our results with literature on HF based electrolytes that also produce hydrogen during electrochemical reduction. We put forth a tentative mechanism for the role of hydrogen, through the combination a LiH containing surface layer, and/or by means of nanobubble templating. Overall, our results provide mechanistic insights on the growth of this particular lithium topography. Further design and control over such columnar lithium metal layers could enable the use of their unique plating/stripping behavior along the length of the column, which can potentially mitigate well-known failure mechanisms of high local current densities and large volumetric changes in lithium metal anodes.

Methods

Equipment

Electrochemical experiments were conducted in an Argon-filled glovebox (MBraun), using an Autolab potentiostat (PGSTAT30) for experiments on stationary electrodes and a Biologic bipotentiostat (VSP-300) for the RRDE experiments. The homemade electrochemical cells

consist of Teflon and include 2 compartments for the reference and counter electrode, respectively, connected by a Luggin capillary. The electrochemical cell was clamped on top of the working electrode sealed and with an O-ring (Kalrez, compound 6375, DuPont) The cells were cleaned using acid piranha (1:3 hydrogen peroxide, 30%, KMG chemicals : Sulfuric acid, 96%, CMC materials) every time a different electrolyte was used, and regularly when using the same electrolyte. Electrolytes were prepared and stored in glassware with a Teflon-coated stirring magnet, all of which were cleaned with acid piranha and brought into the glovebox after vacuum drying at 100° C for several hours before first use.

For the RRDE experiments an MSR rotator was used with an E6R1 ChangeDisk electrode (Cu disk, Pt ring, Pine Research). A glass beaker was used for the RRDE experiments, which was cleaned with acid piranha before every experiment and brought into the glovebox after vacuum drying in the antechamber (no heating). After every experiment the RRDE was polished on a rotating table with a polishing cloth and sequentially using a 3 µm, 1 µm, and 0.25 µm diamond suspension (Dia-complete poly, QATM).

SEM images were made using a NOVA200 near the center of the sample, after cleaving samples in half.

Materials

Sputter-coated copper on silicon wafers was used as a working electrode (150 nm copper + 10 nm titanium on boron doped silicon (ρ = 1-30 Ωm, Si-Mat). Samples were prepared by cleaving the wafer and cleaning with isopropanol. Samples were contacted from the top by folding aluminium foil around the edges, outside the region of the O-ring, which were then placed on a conducting base for contacting the potentiostat. Metallic lithium ribbon was used as counter-, and reference electrodes (99.9%, Sigma-Aldrich), which was scraped clean using a toothbrush before use. Lithium bis(trifluoromethanesulfonyl)imide (LiTFSI, 99.9% under Argon, Solvionic) and $LiClO_4$ (99.99%, battery grade, dry, Sigma-Aldrich) were used as electrolytes in Tetraethylene glycol dimethyl ether (4G, 99%, Sigma-Aldrich), which was dried over 4 Å molecular sieves before use (Thermo Scientific). The water additive was produced at high purity (18.2 MΩ·cm), but stored in a buffertank without a nitrogen blanket. Prior to ex-situ imaging (SEM/AFM) samples were rinsed with Propylene carbonate (99.7% anhydrous, Sigma-Aldrich) and dried in vacuum.

Atomic Force Microscopy

The AFM topography images were obtained using a Bruker Dimension Icon operating in Pulsed Force mode. The AFM tool is located in a N_2/Ar filled glovebox to prevent changes to the sample's surface as result of ambient exposure. All samples were transferred to the AFM glovebox in an airtight sealed container. A HQ-NSC19/AlBs probe with a tip radius of 8 nm and a spring constant of 0.5 N/m was used for the measurements. A low spring constant cantilever is preferred to minimize hard tip-sample interactions to avoid changes to the sample's surface. When Li was present on the sample's surface, a metal coated tip (PPP-EFM) with a tip radius of 25 nm and a spring constant of 2.8 N/m was used instead due to the reactivity of Li with Si and SiN.

Acknowledgements

This work was supported by SIM (Strategic Initiative Materials in Flanders) and VLAIO (Flemish government agency Flanders Innovation and Entrepreneurship) within the SBO project "FuGels" (Grant HBC.2021.0016) in the SIM research program "SIMBA –Sustainable and Innovative Materials for Batteries.

References

1. Tikekar, M. D., Choudhury, S., Tu, Z. & Archer, L. A. Design principles for electrolytes and interfaces for stable lithium-metal batteries. *Nat. Energy* **1**, 16114 (2016).
2. Qian, J. *et al.* High rate and stable cycling of lithium metal anode. *Nat. Commun.* **6**, 6362 (2015).
3. Oyakhire, S. T. *et al.* Electrical resistance of the current collector controls lithium morphology. *Nat. Commun.* **13**, 3986 (2022).
4. Fang, C. *et al.* Pressure-tailored lithium deposition and dissolution in lithium metal batteries. *Nat. Energy* **6**, 987–994 (2021).
5. Liu, Y. *et al.* Insight into the Critical Role of Exchange Current Density on Electrodeposition Behavior of Lithium Metal. *Adv. Sci.* **8**, (2021).
6. Zachman, M. J., Tu, Z., Choudhury, S., Archer, L. A. & Kourkoutis, L. F. Cryo-STEM mapping of solid–liquid interfaces and dendrites in lithium-metal batteries. *Nature* **560**, 345–349 (2018).
7. Xu, G. *et al.* The Formation/Decomposition Equilibrium of LiH and its Contribution on Anode Failure in Practical Lithium Metal Batteries. *Angew. Chemie* **133**, 7849–7855 (2021).
8. Shadike, Z. *et al.* Identification of LiH and nanocrystalline LiF in the solid–electrolyte interphase of lithium metal anodes. *Nat. Nanotechnol.* **16**, 549–554 (2021).
9. Kushima, A. *et al.* Liquid cell transmission electron microscopy observation of lithium metal growth and dissolution: Root growth, dead lithium and lithium flotsams. *Nano Energy* **32**, 271–279 (2017).
10. Yu, S.-H., Huang, X., Brock, J. D. & Abruña, H. D. Regulating Key Variables and Visualizing Lithium Dendrite Growth: An Operando X-ray Study. *J. Am. Chem. Soc.* **141**, 8441–8449 (2019).

11. Cheng, Q. *et al.* Operando and three-dimensional visualization of anion depletion and lithium growth by stimulated Raman scattering microscopy. *Nat. Commun.* **9**, 2942 (2018).
12. Chang, H. J. *et al.* Correlating Microstructural Lithium Metal Growth with Electrolyte Salt Depletion in Lithium Batteries Using 7 Li MRI. *J. Am. Chem. Soc.* **137**, 15209–15216 (2015).
13. Ko, S. *et al.* Electrode potential influences the reversibility of lithium-metal anodes. *Nat. Energy* **7**, 1217–1224 (2022).
14. Bai, P., Li, J., Brushett, F. R. & Bazant, M. Z. Transition of lithium growth mechanisms in liquid electrolytes. *Energy Environ. Sci.* **9**, 3221–3229 (2016).
15. Shi, F. *et al.* Strong texturing of lithium metal in batteries. *Proc. Natl. Acad. Sci.* **114**, 12138–12143 (2017).
16. Ding, F. *et al.* Dendrite-Free Lithium Deposition via Self-Healing Electrostatic Shield Mechanism. *J. Am. Chem. Soc.* **135**, 4450–4456 (2013).
17. Zhang, Y. *et al.* Dendrite-Free Lithium Deposition with Self-Aligned Nanorod Structure. *Nano Lett.* **14**, 6889–6896 (2014).
18. Kanamura, K., Shiraishi, S. & Takehara, Z. Electrochemical Deposition of Uniform Lithium on an Ni Substrate in a Nonaqueous Electrolyte. *J. Electrochem. Soc.* **141**, L108–L110 (1994).
19. Qian, J. *et al.* Dendrite-free Li deposition using trace-amounts of water as an electrolyte additive. *Nano Energy* **15**, 135–144 (2015).
20. Ren, X. *et al.* Guided Lithium Metal Deposition and Improved Lithium Coulombic Efficiency through Synergistic Effects of LiAsF 6 and Cyclic Carbonate Additives. *ACS Energy Lett.* **3**, 14–19 (2018).
21. Mashtalir, O., Nguyen, M., Bodoin, E., Swonger, L. & O'Brien, S. P. High-Purity Lithium Metal Films from Aqueous Mineral Solutions. *ACS Omega* **3**, 181–187 (2018).
22. Chang, W., Park, J. H., Dutta, N. S., Arnold, C. B. & Steingart, D. A. Morphological and Chemical Mapping of Columnar Lithium Metal. *Chem. Mater.* **32**, 2803–2814 (2020).
23. Zhang, X.-Q. *et al.* Columnar Lithium Metal Anodes. *Angew. Chemie* **129**, 14395–14399 (2017).
24. Chang, W., Park, J. H. & Steingart, D. A. Poor Man's Atomic Layer Deposition of LiF for Additive-Free Growth of Lithium Columns. *Nano Lett.* **18**, 7066–7074 (2018).
25. Jo, S. *et al.* The roles of nucleation and growth kinetics in determining Li metal morphology for Li metal batteries: columnar versus spherical growth. *J. Mater. Chem. A* **10**, 5520–5529 (2022).
26. He, Y. *et al.* Understanding the Relationships between Morphology, Solid Electrolyte Interphase Composition, and Coulombic Efficiency of Lithium Metal. *ACS Appl. Mater. Interfaces* **12**, 22268–22277 (2020).
27. Kasse, R. M. *et al.* Understanding additive controlled lithium morphology in lithium metal batteries. *J. Mater. Chem. A* **8**, 16960–16972 (2020).
28. Zhou, J., Chen, J., Yang, J., Nuli, Y. & Wang, J. Dendrite-Free and Micron-Columnar Li Metal Deposited from LiNO3-Based Electrolytes. *ACS Appl. Energy Mater.* **4**, 11336–11342 (2021).
29. Park, M. S. *et al.* A highly reversible lithium metal anode. *Sci. Rep.* **4**, 1–8 (2014).
30. Strmcnik, D. *et al.* Electrocatalytic transformation of HF impurity to H2 and LiF in lithium-ion batteries. *Nat. Catal.* **1**, 255–262 (2018).
31. Langenhuizen, N. P. W. The Effect of Mass Transport on Li Deposition and Dissolution.

J. Electrochem. Soc. **145**, 3094–3099 (1998).
32. Yang, X., Wen, Z., Zhu, X. & Huang, S. Electrodeposition of lithium film under dynamic conditions and its application in all-solid-state rechargeable lithium battery. *Solid State Ionics* **176**, 1051–1055 (2005).
33. Aurbach, D., Daroux, M., Faguy, P. & Yeager, E. The electrochemistry of noble metal electrodes in aprotic organic solvents containing lithium salts. *J. Electroanal. Chem. Interfacial Electrochem.* **297**, 225–244 (1991).
34. Zhang, X. H., Zhang, X., Sun, J., Zhang, Z. & Li, G. Detection of Novel Gaseous States at the Highly Oriented Pyrolytic Graphite - Water Interface. *Langmuir* **23**, 1778–1783 (2007).
35. Seddon, J. R. T. *et al.* Dynamic Dewetting through Micropancake Growth. *Langmuir* **26**, 9640–9644 (2010).
36. Lee, H., Cho, J.-J., Kim, J. & Kim, H.-J. Comparison of Voltammetric Responses over the Cathodic Region in LiPF[sub 6] and LiBETI with and without HF. *J. Electrochem. Soc.* **152**, A1193 (2005).
37. Pei, A., Zheng, G., Shi, F., Li, Y. & Cui, Y. Nanoscale Nucleation and Growth of Electrodeposited Lithium Metal. *Nano Lett.* **17**, 1132–1139 (2017).
38. Biswal, P., Stalin, S., Kludze, A., Choudhury, S. & Archer, L. A. Nucleation and Early Stage Growth of Li Electrodeposits. *Nano Lett.* **19**, 8191–8200 (2019).
39. Zhuang, G., Ross, P. N., Kong, F. & McLarnon, F. The Reaction of Clean Li Surfaces with Small Molecules in Ultrahigh Vacuum: II. Water. *J. Electrochem. Soc.* **145**, 159–164 (1998).
40. Aurbach, D. & Weissman, I. On the possibility of LiH formation on Li surfaces in wet electrolyte solutions. *Electrochem. commun.* **1**, 324–331 (1999).
41. Koshikawa, H. *et al.* Effects of contaminant water on coulombic efficiency of lithium deposition/dissolution reactions in tetraglyme-based electrolytes. *J. Power Sources* **350**, 73–79 (2017).
42. Vilá, R. A. *et al.* LiH formation and its impact on Li batteries revealed by cryogenic electron microscopy. *Sci. Adv.* **9**, eadf3609 (2023).
43. Seddon, J. R. T. & Lohse, D. Nanobubbles and micropancakes: Gaseous domains on immersed substrates. *J. Phys. Condens. Matter* **23**, (2011).
44. Tsai, W. L. *et al.* Building on bubbles in metal electrodeposition. *Nature* **417**, 139–139 (2002).
45. Fan, Y. W. & Wang, R. Z. Submicrometer-Sized Vaterite Tubes Formed Through Nanobubble-Templated Crystal Growth. *Adv. Mater.* **17**, 2384–2388 (2005).
46. Saadat, S. *et al.* Template free electrochemical deposition of ZnSb nanotubes for Li ion battery anodes. *Chem. Commun.* **47**, 9849 (2011).